

SUPPLEMENTAL INFORMATION

**Atmospheric CO₂ estimates for the Miocene to Pleistocene based on foraminiferal $\delta^{11}\text{B}$
at Ocean Drilling Program Sites 806 and 807 in the Western Equatorial Pacific**

Maxence Guillermic^{1,2}, Sambuddha Misra^{3,4}, Robert Eagle^{1,2}, Aradhna Tripathi^{1,2}

¹Department of Atmospheric and Oceanic Sciences, Department of Earth, Planetary, and Space Sciences, Center for Diverse Leadership in Science, Institute of the Environment and Sustainability, University of California – Los Angeles, Los Angeles, CA 90095 USA

²Laboratoire Géosciences Océan UMR6538, UBO, Institut Universitaire Européen de la Mer, Rue Dumont d'Urville, 29280, Plouzané, France

³The Godwin Laboratory for Palaeoclimate Research, Department of Earth Sciences, University of Cambridge, UK

⁴Indian Institute of Science, Centre for Earth Sciences, Bengaluru, Karnataka 560012, India

Supplemental Methods

S1. Potential contamination

We found no evidence for contamination of TE (including Mg/Ca) arising from the presence of silicate minerals or Mn-Fe-Oxide coatings. Contamination of samples by silicate minerals was monitored using Fe/Mg ratios. Samples with Fe/Mg > 0.1 mol/mol are typically rejected due to potential contamination by silicate minerals (Barker et al., 2003). Our samples have an average Fe/Mg of 0.034 ± 0.07 mol/mol (2 SD, n=106), indicating that silicate minerals have been efficiently removed during our cleaning. Contamination by clays was monitored using Ti/Ca no correlations were found between Ti/Ca and Mg/Ca ($R^2=0.0066$) or with B/Ca ($R^2=0.0237$). Contamination by Mn-Fe oxides is detected using Mn/Ca ratios and Fe/Ca ratios. Our samples have Mn/Ca ratios of 0.12 ± 0.11 mmol/mol (2 SD, n=108) consistent with previous published data of cleaned samples (Wara et al., 2005). No correlations was observed between Mg/Ca and Fe/Ca ($R^2=0.0841$) or between Mg/Ca and Mn/Ca ($R^2=0.0161$). No significant correlation was observed between B/Ca and Mn/Ca ($R^2=0.0011$) or B/Ca and Fe/Ca ($R^2=0.0132$) ratios.

S2. Calculations of temperature, salinity, pH, and pCO_2

Analyses of $\delta^{11}B$, $\delta^{18}O$ and elemental ratios (eg., Mg/Ca, B/Ca) were used to reconstruct the chemical and physical properties of seawater over the last 17 My of the Western Equatorial Pacific (Fig. 2).

S2.1. Salinity reconstruction

Salinity was reconstructed using the relative sea level (RSL) reconstruction from Stap et al. (2017) and equation S1:

$$S=S_{\text{modern}}/3800*(3800+RSL) \quad \text{eq. S1}$$

S_{modern} is the modern salinity corresponding to the depth habitat of the foraminifera at the site of interest. The depths used were 125 m for *T. sacculifer* and 80m for *G. ruber* (Rickaby et al., 2005; Guillemic et al., 2020). At Site 806, values for S_{modern} of 35.38 was used for *T. sacculifer* and 35.01 was used for *G. ruber*. At Site 807, a value of 35.05 was used for *T. sacculifer*.

S2.2. Temperature

Paleotemperatures were calculated using Mg/Ca ratios of planktic foraminifera. A number of factors have been shown to impact Mg/Ca ratios and calculated paleotemperature. Factors identified in prior studies include salinity and pH effects on Mg/Ca, seawater Mg/Ca ratios, cleaning methodology, dissolution, and basin-specific equations, as discussed in more detail below. Below we describe some of the prior work that was factored into the regional mono-specific equations we used for calculating temperature from Mg/Ca.

S2.2.1. Prior work showing evidence for salinity and pH effects on Mg/Ca-T

Studies have found that Mg/Ca ratios in foraminifera are impacted by salinity (Nürnberg et al., 1996; Hönisch et al., 2013) and pH or $[\text{CO}_3^{2-}]$ (Russell et al., 2004; Kisakürek et al., 2008; Evans et al., 2016; Gray et al., 2018; Gray and Evans, 2019). Based on culture experiments, Gray and Evans (2019) reported impacts of both salinity and pH on *G. ruber* but only a salinity effect on *T. sacculifer*, and derived the following equations:

$$\text{SST } (T. \text{sacculifer}) = (\text{Ln}(\frac{\text{Mg}}{\text{Ca}} \text{ test}) - 0.054 * (S - 35) + 0.24)/0.062 \quad \text{eq. S2}$$

$$\text{SST } (G. \text{ruber}) = (\text{Ln}(\frac{\text{Mg}}{\text{Ca}} \text{ test} - 0.036 * (S - 35) + 0.87 * (\text{pH} - 8) + 0.03)/0.064 \quad \text{eq. S3}$$

S2.2.2. Prior work showing evidence for variations in Mg/Ca ratios of seawater

Over timescales of 10^6 - 10^7 years, $\text{Mg}/\text{Ca}_{\text{sw}}$ can vary. Evidence from evaporites, carbonate veins, fossil corals and models suggests that seawater $\text{Mg}/\text{Ca}_{\text{sw}}$ ratios have varied through time with variations of ~ 3 mol/mol (Horita et al., 2002; DeFante and Paolo, 2006; Coggon et al., 2011; Brennan et al., 2013; Gothman et al., 2015). These studies do not agree on the timing of changes in $\text{Mg}/\text{Ca}_{\text{sw}}$. To correct for secular variations in $\text{Mg}/\text{Ca}_{\text{sw}}$ we used the approach of O'Brien et al. (2014), theoretical work from Evans and Muller, (2012), and the $\text{Mg}/\text{Ca}_{\text{sw}}$ fourth polynomial equation from Sosdian et al., (2020) derived from calcite veins (Coggon et al., 2010; Rausch et al., 2013), fluid inclusions (Brennan et al., 2013; Horita et al., 2002), echinoderms (Dickson, 2002), and larger benthic foraminifera (Evans et al., 2018). The equations we utilized are adapted from Dekens et al. (2002):

$$\text{SST } (T. \text{sacculifer}) = (\text{Ln}(\frac{\text{Mg}}{\text{Ca}} \text{ test} * \frac{\text{Mg}^H}{\text{Ca}} \text{ sw}_{t0}) - \text{Ln}(0.37 * \frac{\text{Mg}^H}{\text{Ca}} \text{ sw}_t))/0.09 + 0.36 * C + D$$

eq. S4

$$SST(G. ruber) = (Ln(\frac{Mg}{Ca}_{test} * \frac{Mg^H}{Ca} sw_{t0}) - Ln(0.37 * \frac{Mg^H}{Ca} sw_t))/0.09 + 0.61 * C + D \quad \text{eq. S5}$$

Specifically H refers to the power components of the power law relationship between the Mg partition coefficient and Mg/Ca_{sw}, with a value of 0.41 for *T. sacculifer* (Delaney et al., 1985) which we also assume is the same for *G. ruber*. C is the depth of the site. D refer to a basin-specific offset, which is 2 °C for *T. sacculifer* and 2.9 °C for *G. ruber* for the Pacific Ocean, (Table S1).

S2.2.3. Prior work on reductive cleaning effects on Mg/Ca

The use of a reductive step in cleaning has been shown to lower Mg/Ca_{test} ratios in planktic (Barker et al., 2003; Bian et al., 2010; Johnstone et al., 2016) and benthic foraminifera (Yu et al., 2007a), and contribute to offsets between studies using different methodologies. A decrease in Mg/Ca_{test} of 6-9% was reported for *T. sacculifer* by Bian et al. (2010), and of 5% by Johnstone et al. (2016). A decrease of 4% was reported for *G. ruber* by Johnstone et al. (2016).

S2.2.4. Mg/Ca-SST equations used for this study

Based on the above equations from Gray and Evans (2019) (eq. S2 and S3), we incorporated a term to account for changes in the Mg/Ca ratio of seawater, and based on results from Dekens et al., (2002) we incorporated two terms to account for dissolution (C) and basin-specific offsets (D), and used an iterative approach for our calculations to account for pH effect on *G. ruber* (Gray and Evans, 2019). The equations we used are:

$$SST(T. sacculifer) = \frac{Ln\left(\frac{Mg}{Ca}_{test} * 1.05 * \frac{\frac{Mg^H}{Ca} sw_{t0}}{\frac{Mg^H}{Ca} sw_t}\right) - 0.054 * (S - 35) + 0.24}{0.062} + 0.36 * C + 2.0 \quad \text{eq. S6}$$

$$SST(G. ruber) = \frac{Ln\left(\frac{Mg}{Ca}_{test} * 1.05 * \frac{\frac{Mg^H}{Ca} sw_{t0}}{\frac{Mg^H}{Ca} sw_t}\right) - 0.036 * (S - 35) + 0.87 * (pH - 8) + 0.03}{0.064} + 0.61 * C + 2.9 \quad \text{eq. S7}$$

With H being the power components of the power relationship between the Mg partition coefficient and Mg/Ca_{sw}, 0.41 for *T. sacculifer* (Delaney et al., 1985). We use the same value

for *G. ruber*. C is the depth of the core (km). In order to take the impact of reductive cleaning into account we applied a decrease of 5% for *G. ruber* and *T. sacculifer* (Bian et al., 2010 and Johnstone et al., 2016).

Given evidence for a pH effect on Mg/Ca-SST calibration for *G. ruber*, we used an iterative approach for our calculations, following Gray and Evans, (2019). Up to 4 iterations were needed to achieve a difference in SST with the previous iteration of $<0.05^{\circ}\text{C}$ and a difference in pH of <0.001 . For this iterative approach, we first calculate pH_1 from foraminiferal $\delta^{11}\text{B}$, then calculate SST_1 from pH_1 , then calculate pH_2 with SST_1 , and then repeat.

S2.3. $\delta^{11}\text{B}_{\text{borate}}$ from $\delta^{11}\text{B}_{\text{carbonate}}$

The use of $\delta^{11}\text{B}$ in foraminiferal carbonate to calculate seawater $\delta^{11}\text{B}_{\text{borate}}$, and derived pH and pCO_2 values, has been shown to accurately replicate pCO_2 records independently determined from ice cores and using oceanographic data, if several factors are taken into account (Chalk et al., 2017; Guillermic et al., 2020). These factors include mono-specific calibrations, size fraction or shell weight, basin, and water depth. In order to accurately reconstruct seawater pH (and pCO_2) from $\delta^{11}\text{B}$ of foraminifera, mono-specific calibrations are needed to convert $\delta^{11}\text{B}_{\text{carbonate}}$ to $\delta^{11}\text{B}_{\text{borate}}$. Recent culture and field-based calibrations have refined the sensitivities of $\delta^{11}\text{B}_{\text{carbonate}}$ to $\delta^{11}\text{B}_{\text{borate}}$ for different foraminiferal species (Henahan et al., 2016; Raitzsch et al., 2018; Guillermic et al., 2020). For *T. sacculifer* and *G. ruber*, the sensitivities of $\delta^{11}\text{B}_{\text{carbonate}}$ to $\delta^{11}\text{B}_{\text{borate}}$ are 0.82 and 0.58, respectively (Raitzsch et al., 2018; Guillermic et al., 2020). As with Mg/Ca, the intercepts are prone to large uncertainties and are commonly adjusted based on core-top data, in order to yield the expected pre-industrial pH or pCO_2 value at the site being examined (Chalk et al., 2017; Sosdian et al., 2018). The rationale for this correction is the impact of the depth habitat on microenvironment pH and subsequent $\delta^{11}\text{B}_{\text{carbonate}}$ (Hönisch and Hemming, 2004; Guillermic et al., 2020) and/or preferential dissolution of gametogenic calcite (Ni et al., 2007). It is also possible that these offsets may reflect observed size effects on *G. ruber* as well as *T. sacculifer* (Henahan et al., 2013; Hönisch et al., 2019). For *T. sacculifer*, a relationship between shell size and $\delta^{11}\text{B}_{\text{carbonate}}$ has been observed in the WEP (Hönisch and Hemming, 2004; Ni et al., 2007). Hönisch and Hemming, (2004) also reported that values for the 515-865 μm size fraction yielded values of 21.76 ‰, and determined a size-fraction specific relationship. Here, we modify this approach to develop a shell-weight specific relationship:

$$\text{Size offset (\%)} = 21.76 - (0.06522 * \text{Weight/shell } (\mu\text{g}) + 17.38) \quad \text{eq. S8}$$

We adapted the equation for *T. sacculifer* from Guillermic et al. (2020):

$$\delta^{11}\text{B}_{\text{borate}} = [(\delta^{11}\text{B}_{T. \text{sacculifer}} + \text{Size offset}) - 4.09 (\pm 0.86)] / 0.83 (\pm 0.48) \quad \text{eq. S9}$$

Due to the lack of coretop measurements for *G. ruber* from this study, we selected three control points at Marine isotope stages (MIS) 30, 37 and 39 (Lisiecky and Raymo, 2005) times when both *T. sacculifer* and *G. ruber* were measured to determine appropriate offsets for both Mg/Ca and $\delta^{11}\text{B}$ that yield (Table S1 and S2) the best agreement between the species. This was used to adapt the equation from Guillermic et al. (2020) for *G. ruber*:

$$\delta^{11}\text{B}_{\text{borate}} = [(\delta^{11}\text{B}_{G. \text{ruber}} + 2.0) - 9.11 (\pm 0.73)] / 0.58 (\pm 0.91) \quad \text{eq. S10}$$

S2.4. Constants

Temperature, salinity and pressure were used to calculate the different dissociation constants and parameters. We used K_1 , K_2 from Lueker et al. (2000), K_B from Dickson, (1990), KSO_4 from Dickson, (1990), KF from Peres and Fraga, (1987) and total boron from Lee et al. (2010).

S2.5. pH calculations

The quantitative estimation of pH using downcore $\delta^{11}\text{B}_{\text{carbonate}}$ requires: 1) calculations of the borate isotopic composition of seawater ($\delta^{11}\text{B}_{\text{borate}}$), 2) constraints on the secular variation of the boron isotopic composition of seawater ($\delta^{11}\text{B}_{\text{seawater}}$), 3) the fractionation factor (α) between $\text{B}(\text{OH})_3$ and $\text{B}(\text{OH})_4^-$ and 4) the calculations of acid/base equilibrium constants based temperature, salinity and pressure. To translate our $\delta^{11}\text{B}$ measurements to pH, we used the following relationship (Hemming and Hanson, 1992):

$$\text{pH} = \text{pK}_B^* - \log \left(\frac{\delta^{11}\text{B}_{\text{seawater}} - \delta^{11}\text{B}_{\text{borate}}}{\delta^{11}\text{B}_{\text{seawater}} - \alpha * \delta^{11}\text{B}_{\text{borate}} - \varepsilon} \right) \quad \text{eq. S11}$$

pK_B^* is the dissociation constant between the two boron species (8.5975 at 25 °C and a salinity of 35 psu, Dickson, 1990). A fractionation between $\text{B}(\text{OH})_3$ and $\text{B}(\text{OH})_4^-$ (ε) of $27.2 \pm 0.6 \text{ ‰}$ was empirically determined by Klochko et al. (2006) in seawater and confirmed independently using a different method by Nir et al. (2015).

A few studies have attempted to reconstruct secular variations of $\delta^{11}\text{B}_{\text{seawater}}$ (Lemarchand et al., 2000; Foster et al., 2012; Raitzsch and Hönisch, 2013; Greenop et al., 2017). For our work, we first compared different scenarios (Fig. 3). These scenarios are modeled values of $\delta^{11}\text{B}_{\text{seawater}}$ based on constraints on the boron budget from Lemarchand et al. (2000), a second modeled history that assumed changes in seawater pH from Raitzsch and Hönisch (2013), and a third scenario that also considered constraints on pH gradients from $\delta^{13}\text{C}$ measurements published by Greenop et al. (2017).

S2.6. pCO₂ calculations

The carbonate system has two degrees of freedom, meaning that if two parameters of the carbonate system are known all the others can be calculated. For this study, we utilized pH calculated using $\delta^{11}\text{B}_{\text{borate}}$, and total alkalinity (TA) as a second parameter that are shown in Fig. 3-4. We used four different alkalinity scenarios for our calculations (Constant alkalinity; Tyrell and Zeebe, 2004; Ridgwell and Zeebe, 2005; and Caves et al. 2016). For all calculations, we used the MS excel program “CO₂sys” version 2.3 from Pierrot et al. (2006). pH and TA, temperature, salinity were used to determined pCO₂ in ppm.

S2.7. Error propagation for temperature (T), pH and pCO₂

The main source of uncertainty in reconstructed pCO₂ comes from the errors in pH. Table S3 summarizes the sensitivity of pH and pCO₂ to different variables. The individual uncertainties were propagated in quadrature to combined uncertainties for temperature (δT), pH (δpH) and pCO₂ (δpCO_2) (eq. S12, S13, S14, S15, S16 and S17). Minimum and maximum propagated uncertainties were derived separately for pH and pCO₂. δpCO_2 (A) is the full uncertainty propagation, δpCO_2 (B) is the uncertainty propagation without taking into account the $\delta^{11}\text{B}_{\text{sw}}$. Both are shown in the figures and discussed below.

$$\delta T_{G. \text{ruber}} = \sqrt{(\delta T_{\text{Mg/Ca}})^2 + (\delta T_{\text{Salinity}})^2 + (\delta T_{\text{pH}})^2} \quad \text{eq. S12}$$

$$\delta T_{T. \text{sacculifer}} = \sqrt{(\delta T_{\text{Mg/Ca}})^2 + (\delta T_{\text{Salinity}})^2} \quad \text{eq. S13}$$

$$\delta pH (A) = \sqrt{(\delta pH_Temperature)^2 + (\delta pH_Salinity)^2 + (\delta pH_^{11}B_{sw})^2 + (\delta pH_^{11}B_{carbonate})^2}$$

eq. S14

$$\delta pH (B) = \sqrt{(\delta pH_Temperature)^2 + (\delta pH_Salinity)^2 + (\delta pH_^{11}B_{carbonate})^2} \quad \text{eq. S15}$$

$$\delta pCO_2 (A) = \sqrt{\frac{(\delta pCO_2_Temperature)^2 + (\delta pCO_2_Salinity)^2 + (\delta pCO_2_^{11}B_{sw})^2 + (\delta pCO_2_^{11}B_{carbonate})^2 + (\delta pCO_2_Alkalinity)^2}{}} \quad \text{eq. S16}$$

$$\delta pCO_2 (B) = \sqrt{\frac{(\delta pCO_2_Temperature)^2 + (\delta pCO_2_Salinity)^2 + (\delta pCO_2_^{11}B_{carbonate})^2 + (\delta pCO_2_Alkalinity)^2}{}} \quad \text{eq. S17}$$

With for example, “ $\delta pCO_2_Temperature$ ” being the uncertainty in pCO_2 due to temperature.

Figures

Figure S1: Evaluation of pCO₂ reconstruction for the past 0.8 million year in the Western Equatorial Pacific compared to benthic oxygen isotope data. **A.** Benthic $\delta^{18}\text{O}$ (blue line – stack from Lisiecki and Raymo, 2005; black line – compilation from Zachos et al., 2008). **B to E**, colored is indicating the site (filled light blue=806, filled dark blue=807), symbols represent the species (circle=*T. sacculifer* and triangle=*G. ruber*), filled grey squares are recalculated data based on Sosdian et al. (2018) at site 872. Reconstructed pCO₂ (ppm) using boron-based pH and alkalinity from Caves et al. (2016), data presented are from this study. Propagated uncertainties are given by eq. S17 for the dark blue envelope, while the light blue envelope are the uncertainties calculated based on eq. S16 (taking into account uncertainty on $\delta^{11}\text{B}_{\text{seawater}}$). Solid black line represents data from ice cores (Bereiter et al., 2015). **B.** Colored data from this study. **C.** Colored data from this study and pCO₂ from original publications. **D.** Colored data from this study and data recalculated by Rae et al. (2021). **E.** Colored data from this study and data recalculated by Sosdian et al. (2018).

Figure S2: Evaluation of pCO₂ reconstruction for the past 22 million years in the Western Equatorial Pacific compared to benthic oxygen isotope data. **A.** Benthic $\delta^{18}\text{O}$ (blue line – stack from Lisiecki and Raymo, 2005; black line – compilation from Zachos et al., 2008). **B to E**, colored is indicating the site (filled light blue=806, filled dark blue=807), symbols represent the species (circle=*T. sacculifer* and triangle=*G. ruber*), filled grey squares are recalculated data based on Sosdian et al. (2018) at site 872. Reconstructed pCO₂ (ppm) using boron-based pH and alkalinity from Caves et al. (2016), data presented are from this study. Propagated uncertainties are given by eq. S17 for the dark blue envelope, while the light blue envelope are the uncertainties calculated based on eq. S16 (taking into account uncertainty on $\delta^{11}\text{B}_{\text{seawater}}$). Solid black line represents data from ice cores (Bereiter et al., 2015). **B.** Colored data from this study. **C.** Colored data from this study and pCO₂ from original publications. **D.** Colored data from this study and data recalculated by Rae et al. (2021). **E.** Colored data from this study and data recalculated by Sosdian et al. (2018).

Tables

Table S1: Control points for a 2‰ offset used for *G. ruber*.

Table S2: Comparison of the control points reconstructions between *T. sacculifer* and *G. ruber* for MIS 30, 37 and 39, using different offsets (see text).

Table S3: Sensitivity tests for reconstructed pH and pCO₂ (G17, Caves-16), all results are given as the minimum and maximum variation (%) observed in our data.

Table S4: Boron isotopes standard reproducibility.

Table S5: CamWuellesstorfi, X/Ca standard reproducibility.

Table S1: Control points for a 2‰ offset used for *G. ruber*

	Species	Sample			med	mbsf	Shell Wt (µg)	Age (Ma)	SST (°C)	error (°C)	Salinity (psu)	TA (µmol/kg)	pH (total scale)	error(1) up	pCO ₂ (ppm)	error(1) up (ppm)	error(1) down (ppm)		
MIS 30	<i>G. ruber</i>	806	B 3	5	6	8	22.06	22.06	16.1	1.046	26.2	1.8	35.3	2241	8.16	0.09	258	74	57
	<i>T. sacculifer</i>	806	B 3	5	31	33	22.31	22.31	18.2	1.048	26.0	0.9	35.6	2230	8.28	0.08	174	47	37
	<i>G. ruber</i>	806	B 4	1	71	73	26.21	26.21	17.0	1.240	26.4	1.9	35.1	2230	8.09	0.09	318	96	72
MIS 37	<i>T. sacculifer</i>	806	B 4	1	56	58	26.06	26.06	22.2	1.233	29.8	0.9	35.6	2228	8.08	0.09	308	91	69
	<i>G. ruber</i>	806	B 4	1	131	133	26.81	26.81	16.1	1.267	27.8	1.9	35.5	2228	8.09	0.09	320	95	71
	<i>T. sacculifer</i>	806	B 4	1	146	148	26.96	26.96	24.0	1.274	27.8	0.9	35.6	2219	8.07	0.09	319	97	72
MIS 39	<i>G. ruber</i>	806	B 4	1	131	133	26.81	26.81	16.1	1.267	27.8	1.9	35.5	2228	8.09	0.09	320	95	71
	<i>T. sacculifer</i>	806	B 4	1	146	148	26.96	26.96	24.0	1.274	27.8	0.9	35.6	2219	8.07	0.09	319	97	72

Table S2: Comparison of the control points reconstructions between *T. sacculifer* and *G. ruber* for MIS 30, 37 and 39, using different offsets (see text).

	1.8 ‰ offset			1.85 ‰ offset			2.0 ‰ offset			2.1 ‰ offset		
	MIS 30	MIS 37	MIS 39	MIS 30	MIS 37	MIS 39	MIS 30	MIS 37	MIS 39	MIS 30	MIS 37	MIS 39
ΔpCO ₂ (ppm)	105	37	26	100	31	20	86	13	2	77	1	-10
ΔpH (tot scale)	-0.14	-0.02	-0.01	-0.14	-0.01	-0.003	-0.12	0.01	0.02	-0.11	0.02	0.03
ΔT (°C)	-0.02	-3.75	-0.36	0.06	-3.65	-0.27	0.31	-3.39	-0.005	0.47	-3.21	0.17

Table S3: Sensitivity tests for reconstructed pH and pCO₂ (G17, Caves-16), all results are given as the minimum and maximum variation (%) observed in our data

	Salinity	Temperature	δ ¹¹ B _{carbonate}	δ ¹¹ B _{seawater}	Alkalinity
pH (<i>G. ruber</i>)	0.07%	0.2-0.3%	0.2-0.5 %	0.8-1.6 %	NA
pH (<i>T. sacculifer</i>)	0.07-0.08 %	0.12-0.13 %	0.1-0.5 %	0.8-1.4 %	NA
pCO ₂ (<i>G. ruber</i>)	0.8-1.5 %	0.02-1.5 %	5-11 %	19-25 %	5 %
pCO ₂ (<i>T. sacculifer</i>)	0.8-1.4 %	0.02-0.7 %	3-12 %	19-27 %	5-7 %

NA: non determined parameter

Table S4: Boron isotopes standard reproducibility.

Standard	$\delta^{11}\text{B}_1$ (‰)	$2\text{SD}_{\text{AEI21}}$	n_{AEI21}	$\delta^{11}\text{B}_2$ (‰)	$2\text{SD}_{\text{AEI21}}$	n_{AEI21}
NEP1	25.36	0.36	11	25.32	0.36	11
NEP2	25.21	0.25	11	25.22	0.25	11
NEP3	25.00	0.30	12	24.70	0.30	12
NEP4	25.40	0.21	11	25.32	0.21	11
NEP5	25.33	0.21	11	25.22	0.21	11
NEP7	25.26	0.26	15	25.39	0.26	15
NEP8	26.15	0.26	15	25.97	0.26	15
NEP9	26.09	0.26	15	26.09	0.26	15
NEP10	26.22	0.26	15	26.29	0.26	15
NEP11	26.19	0.26	15	26.21	0.26	15
NEP12	26.12	0.26	15	26.13	0.26	15
NEP13	26.00	0.26	15	26.04	0.26	15
NEP15	26.02	0.29	12			
NEP16	25.86	0.29	12			
NEP17	25.83	0.19	3	25.49	0.33	8
NEP18	25.72	0.19	3	26.03	0.33	8
NEP19	26.48	0.33	8	26.06	0.33	8
NEP20	25.82	0.27		25.50	0.27	
NEP21	25.42	0.15	3			
NEP22	25.28	0.29	8			
NEP23	25.32	0.15	3	25.34	0.29	8
NEP24	25.27	0.29	8	25.47	0.29	8
NEP25	25.54	0.22	6			
NEP26	25.86	0.22	4	25.95	0.22	4
NEP27	26.16	0.22	6	26.42	0.22	6
NEP28	25.77	0.25	9			
NEP29	25.37	0.22	4			
NEP30	25.88	0.25	9			
NEP31	25.46	0.22	4			
NEP32	25.93	0.25	9			
NEP33	26.41	0.22	4	26.21	0.22	4
JCP-1-1	24.07	0.10				
JCP-1-2	24.17	0.11		24.17	0.10	
JCP-1-3	24.01	0.11				
JCP-1-4	23.92	0.26				
JCP-1-5	24.03	0.26		24.05	0.39	
JCP-1-6	24.18	0.36		24.16	0.36	
Standard	Average $\delta^{11}\text{B}$	2SD	n			
NEP	25.72	0.79	31	This study		
NEP	26.20	0.88	27	Holcomb et al. 2015		
NEP	25.80	0.89	6	Sutton et al. 2017		
JCP-1	24.06	0.19	6	This study		
JCP-1	24.37	0.32	57	Holcomb et al. 2015		
JCP-1	24.42	0.28	7	Sutton et al. 2017		

*Some data in this table are also presented in Guillermic et al. 2021 because data were collected at the same period

Table S5: CamWuellerstorfi, X/Ca standard reproducibility

Sample	Li/Ca μmol/mol	B/Ca μmol/mol	Mg/Ca mmol/mol	Sr/Ca mmol/mol	Cd/Ca μmol/mol	Ba/Ca μmol/mol	U/Ca nmol/mol	Mn/Ca μmol/mol	Fe/Ca mmol/mol
CamWuellerstorfi	16.0	204	1.22	1.31	0.26	4.6	43	67	0.04
CamWuellerstorfi	16.3	209	1.24	1.32	0.28	4.6	45	69	0.04
CamWuellerstorfi	16.3	209	1.23	1.31	0.26	4.6	44	77	0.04
CamWuellerstorfi	16.0	207	1.23	1.32	0.28	4.6	44	74	0.04
CamWuellerstorfi	16.4	210	1.23	1.32	0.27	4.6	42	74	0.04
CamWuellerstorfi	16.0	208	1.24	1.31	0.26	4.6	42	74	0.04
CamWuellerstorfi	16.6	213	1.23	1.32	0.28	4.6	44	74	0.04
CamWuellerstorfi	16.0	203	1.22	1.32	0.26	4.6	41	72	0.04
CamWuellerstorfi	16.1	205	1.22	1.32	0.27	4.6	42	76	0.04
CamWuellerstorfi	16.2	204	1.22	1.32	0.27	4.6	41	72	0.04
CamWuellerstorfi	16.1	205	1.22	1.32	0.27	4.5	41	71	0.04
CamWuellerstorfi	15.8	204	1.21	1.32	0.27	4.6	42	73	0.04
CamWuellerstorfi	16.1	206	1.22	1.32	0.27	4.6	42	68	0.04
CamWuellerstorfi	16.0	207	1.22	1.32	0.26	4.6	43	66	0.04
CamWuellerstorfi	15.9	203	1.21	1.32	0.27	4.6	42	68	0.04
CamWuellerstorfi	16.3	201	1.22	1.31	0.22	4.6	41	66	0.03
CamWuellerstorfi	16.1	203	1.22	1.32	0.23	4.6	42	67	0.03
CamWuellerstorfi	16.4	202	1.22	1.32	0.23	4.6	42	69	0.04
CamWuellerstorfi	16.3	202	1.22	1.31	0.22	4.6	41	68	0.04
CamWuellerstorfi	16.6	202	1.22	1.31	0.23	4.6	44	67	0.03
CamWuellerstorfi	16.6	205	1.22	1.31	0.24	4.5	42	66	0.03
CamWuellerstorfi	16.1	204	1.22	1.31	0.22	4.6	40	67	0.03
CamWuellerstorfi	16.4	204	1.22	1.31	0.23	4.6	43	67	0.03
CamWuellerstorfi	16.4	202	1.22	1.32	0.23	4.6	43	64	0.03
CamWuellerstorfi	16.2	198	1.22	1.31	0.31	4.6	42	74	0.04
CamWuellerstorfi	16.4	200	1.22	1.30	0.30	4.6	43	73	0.04
CamWuellerstorfi	16.2	201	1.23	1.31	0.31	4.7	43	74	0.04
CamWuellerstorfi	16.3	198	1.22	1.31	0.30	4.6	42	73	0.04
CamWuellerstorfi	16.6	200	1.23	1.30	0.30	4.6	42	73	0.04
CamWuellerstorfi	16.5	198	1.22	1.31	0.31	4.6	44	74	0.04
CamWuellerstorfi	16.1	201	1.22	1.30	0.32	4.7	43	74	0.04
CamWuellerstorfi	16.5	197	1.25	1.31	0.29	4.9	43	72	0.04
CamWuellerstorfi	16.6	197	1.25	1.32	0.29	4.8	44	74	0.04
CamWuellerstorfi	16.8	196	1.25	1.32	0.29	4.9	44	72	0.04
CamWuellerstorfi	17.0	198	1.25	1.32	0.28	4.9	44	71	0.04
CamWuellerstorfi	16.8	198	1.25	1.31	0.29	4.9	44	73	0.04
CamWuellerstorfi	16.5	198	1.25	1.31	0.29	4.9	43	72	0.04
CamWuellerstorfi	16.7	200	1.24	1.32	0.29	4.9	43	74	0.04
CamWuellerstorfi	16.9	202	1.24	1.31	0.29	4.9	43	74	0.04
Average	16.3	203	1.23	1.31	0.27	4.7	43	71	0.04
2SD	0.6	8	0.02	0.01	0.05	0.2	2	7	0.01
n	39	39	39	39	39	39	39	39	39

*Some data in this table are also presented in Guillermic et al. 2021 because data were collected at the same period

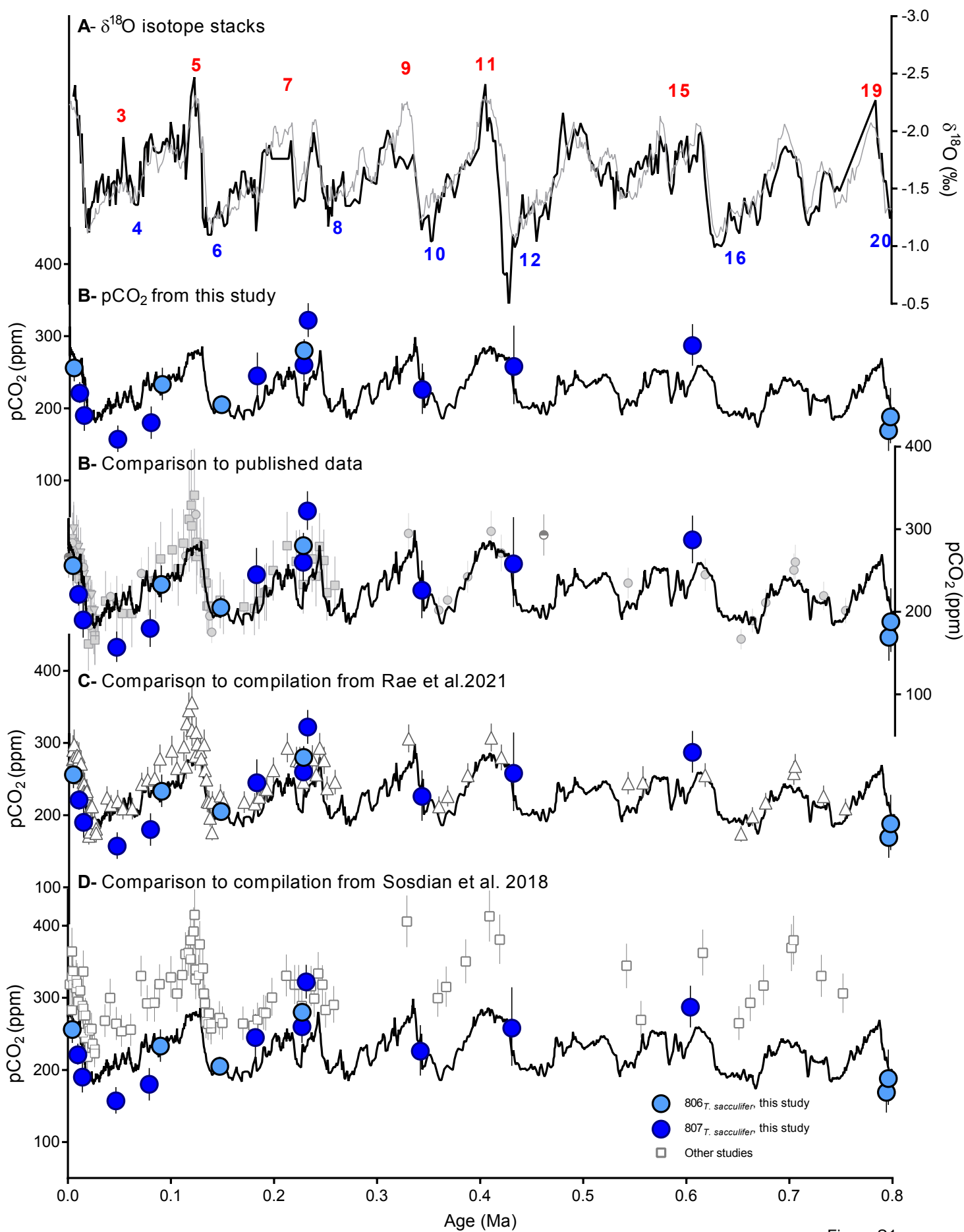


Figure S1

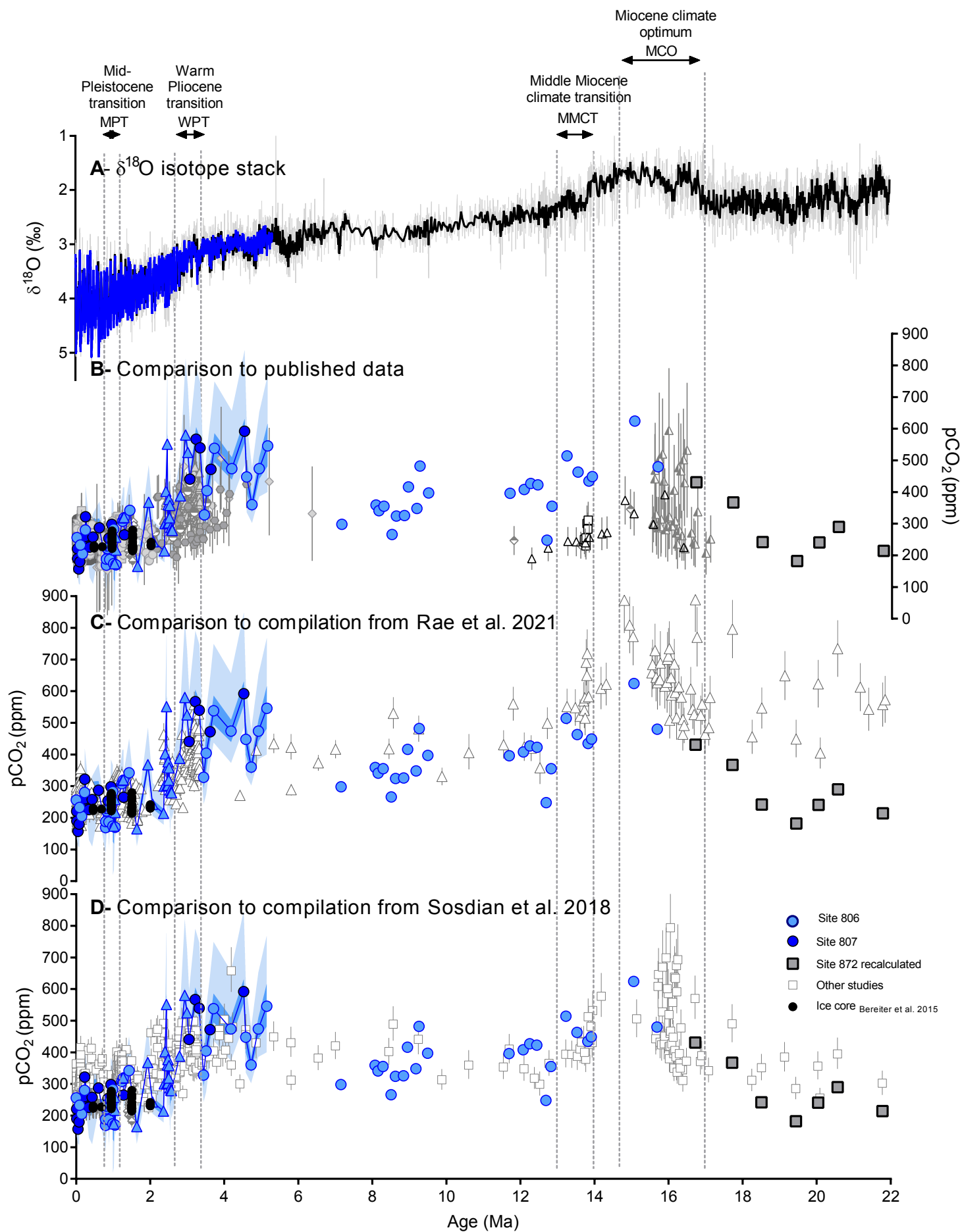


Figure S2